Equilibrium Core Modeling of a Pebble Bed Reactor Similar to the Xe-100 with SCALE

Annie Berens[1], Friederike Bostelmann[2], Nicholas R. Brown[1,*]

[1] *University of Tennessee, Knoxville, 863 Neyland Drive, Knoxville, TN 37996*
[2] *Oak Ridge National Laboratory, One Bethel Valley Road, Oak Ridge, TN 37830*

* Corresponding author: Nicholas R. Brown, nbrown49@utk.edu

Keywords: HTGR; pebble bed; SCALE; equilibrium core; Xe-100

Abstract

As the nuclear industry moves towards licensing and constructing advanced reactors, new attention has been focused on the advanced reactor designs that have past operational experience, such as pebble-bed high-temperature gas-cooled reactors (PB-HTGRs). Pebble-bed reactor designs have many advantages, such as their higher operating temperatures and online refueling capabilities. However, high-fidelity computational modeling of pebble-bed reactor designs, from reactor startup to operation at equilibrium, is more challenging compared to conventionally fueled reactors due to the continuous movement of the fuel pebbles through the reactor during operation. In previous work at Oak Ridge National Laboratory (ORNL), the SCALE Leap-In method for Cores at Equilibrium (SLICE) was developed around tools within the SCALE code system. This iterative method can effectively generate pebble-bed reactor zone-wise fuel inventories at equilibrium core operation within a reasonable computational time. The objective of this work was to further verify the ORNL SLICE method and to investigate the impact of considering temperature profiles during the application of the method. The SLICE method was applied to a modular high-temperature gas-cooled reactor design based upon publicly available design specifications of the Xe-100 pebble-bed reactor. Upon comparing the results from the SLICE method to published literature, the differences in the eigenvalue $k_{effective}$ were on the order of several hundred pcm (percent millirho). To investigate one possible cause of these differences, a study looking at the sensitivity of the full-core equilibrium $k_{effective}$ and discharge nuclide inventory to temperature was performed by developing equilibrium cores of two additional temperature profiles. From this temperature study, differences on the order of hundreds of pcm for the full-core equilibrium $k_{effective}$, and up to 15% difference for the discharge inventories were found. These results indicated the strong dependence on temperature that needs to be considered for future work in equilibrium modeling of PB-HTGRs.

1. Introduction

Leveraging past operational experience, intrinsic safety features, and potential process heat and cogeneration applications, pebble-bed high-temperature gas-cooled reactors (PB-HTGRs) are one of the most promising fourth generation reactor concepts (Kadak, 2005). PB-HTGRs have a cylindrical core region that contains fuel pebbles surrounded by helium coolant gas. Fuel pebbles enter the core through a fuel chute at the top and exit the core through a fuel chute at the bottom. The fuel pebbles are typically spherical graphite elements that have a central

graphite matrix region in which tri-structural (TRISO) fuel particles are embedded. Pebble movement through the reactor is driven by gravity, and pebbles are typically recirculated through the reactor several times, depending on the design. Moderation in the reactor is provided by both the graphite material of the pebbles and the graphite reflector that surround the core. PB-HTGR designs include a variety of intrinsic safety features, such as large negative temperature coefficients of reactivity, and can potentially be used for process heat and cogeneration applications. Unlike other fourth generation reactor designs, PB-HTGRs have years of operational experience with both commercial and experimental PB-HTGRs. This experience has helped guide the design of PB-HTGRs in a direction that lends to future commercial feasibility of this new fourth generation concept.

1.1 Past, Current, and Proposed PB-HTGRs

Two PB-HTGRs, the Arbeitsgemeinschaft Versuchsreaktor (AVR) (Krüger et al., 1988) and the Thorium-High-Temperature-Reactor (THTR-300) (Bäumer et al., 1990), were constructed and operated in Germany between 1967 and 1988. The AVR was a 15 Mwe experimental reactor that was used to study the operation of a pebble-bed reactor (PBR) in both steady-state and transient conditions and was utilized for a variety of in-pile testing and experiments (Krüger et al., 1988). The 300 MWe thorium fueled THTR-300 PBR was designed to be a scaled-up version of the AVR, utilizing many of the lessons learned from the AVR within the design (Bäumer et al., 1990). Both the AVR and the THTR-300 proved the feasibility of a PB-HTGR design and provided valuable insight for future PB-HTGR designs, such as the HTR-10 and the HTR-PM in China. The HTR-10 is a 10 MWe experimental PB-HTGR whose design and operation allowed for the validation of modern PBR modeling codes, such as the Physical Analysis code of General Utility (PANGU) (She et al., 2021; She et al., 2019). The HTR-PM is a currently operating commercial two module 211 MWe PB-HTGR (Jian et al., 2014). There are several U.S. based companies proposing PBRs, leveraging many of the lessons learned from previous PBRs in their designs. Designed by X-Energy, the Xe-100 is a 200 MWth helium cooled PB-HTGR that utilizes a multipass refueling scheme (Mulder & Boyes, 2020). The combination of the intrinsic safety features and economic viability of the Xe-100 make it an attractive reactor design that has already been selected by DOW chemicals for placement at one of their Gulf Coast sites by the 2030's (DOW, 2022).

1.2 Computational Modeling of PBRs

Computational modeling of PBRs plays an important role in verifying the safe operation of the aforementioned reactors under normal and accidents conditions. However, the modeling is challenging due to the complex geometry and the continuous circulation of the fuel pebbles through the core. One of the goals of PBR modeling is to generate a computational model of the reactor during operation at equilibrium. The operating cycle of a PBR begins with the reactor core in an initial criticality configuration. In this configuration, the core is typically filled with a combination of fueled and unfueled, or dummy, graphite pebbles. After initial criticality is reached, pebble circulation begins with both fueled and dummy pebbles circulating in and out of the core. The dummy pebbles are gradually replaced by fuel pebbles, and eventually the core will contain only fuel pebbles that have passed through the core a varying number of times, thus having different burnups and containing different nuclide inventories. At the point at which the

conditions in the individual core regions, such as the region-average nuclide inventory, are approximately constant over time, an equilibrium core has been reached. An accurate calculation of a PBR core at equilibrium is crucial for a variety of analyses, such as understanding the expected inventory of pebbles discharged from the reactor for the purpose of storage and potential recycling.

Currently, two general strategies for the computational modeling of an equilibrium core exist. The first is the "run-in" method, which begins with the initial critical configuration of the core and models the core's evolution from initial criticality to equilibrium. This approach is used in codes such as Very Special Old Programs (VSOP) (Teuchert et al., 1980) and PANGU (She et al., 2019). The second approach is the "jump-in" method, which does not attempt to model the "run-in" of the core to equilibrium. Instead, modelling begins with a core that contains only fueled pebbles, and iterative updates of the cross-sections and nuclide inventory are performed until the convergence of target quantities is reached. The PEBBED code and the *kugelpy* python wrapper are examples of codes that utilize this modeling strategy (Skutnik & Wieselquist, 2021; Stewart et al., 2024).

Results from two previous studies on the neutronics of the Xe-100 were used as a basis of comparison for this work. The first study by Mulder and Boyes is an analysis with VSOP-A (Mulder & Boyes, 2020). VSOP-A is a "run-in" modeling code that is able to simulate a high-temperature gas cooled reactor from initial criticality to equilibrium through numerical simulations of neutron diffusion, fuel burnup, shuffling, and reactor control in either 2 or 3D using the ENDF/B-VII data library (Lu & Wu, 2022; Mulder & Boyes, 2020). Additionally, it can perform thermo-fluid dynamics in 2D, fuel cycle cost calculations, and the simulation of quasi steady-state transients like depressurized or pressurized loss of force cooling (Mulder & Boyes, 2020). The second study is an analysis with the Methodology to Effectively Estimate the Equilibrium State of a PBR (MEEES-PBR) (Lu & Wu, 2022). MEEES-PBR is an equilibrium method developed at Virginia Commonwealth University (VCU) that utilizes the Serpent Monte Carlo (MC) code for both transport and depletion calculations (Leppänen, 2013). The MEEES-PBR method starts with the construction of a high-fidelity MC model of the Xe-100, that initially contains only fresh fuel. The core is then divided into a number of fuel regions and the expected burnup is calculated for each. A depletion calculation is then performed and a multifuel region model is developed using the outputted isotopic compositions for each fuel region. If the resulting $k_{effective}$ is within the specified tolerance of the equilibrium state, equilibrium is considered to have been reached. Otherwise, the burnup of the feeding pebbles is updated and the process repeats starting with the calculation of the burnup within each fuel region (Lu & Wu, 2022).

The equilibrium modeling method used for this work is the SCALE Leap-In method for Cores at Equilibrium (SLICE) developed at Oak Ridge National Laboratory (ORNL) (Bostelmann et. al, 2022) that utilizes neutron transport and depletion capabilities of the SCALE code system (Wieselquist & Lefebvre, 2023). Similar to the aforementioned approaches, this method iterates between MC neutron transport and depletion calculations until convergence of target quantities including $k_{effective}$ and specific nuclide concentrations is reached. However, rather than running computationally intense full-core depletion calculations, detailed depletion calculations are performed using a model of a 2D axial slice through the reactor core with axially reflective boundary conditions. The use of the slice model rather than a full-core model for equilibrium core generation purposes is justified for large PBR cores because radial effects dominate the neutron spectrum's characteristics, whereas axial effects are of secondary

importance (Skutnik & Wieselquist, 2021). Using this smaller model allows for the reduction of the computational resources required compared to a full-core model. The purpose of this method is not to generate a high-fidelity equilibrium model, but rather generate an approximation to the equilibrium core of the reactor. The SLICE method has been applied previously to the modeling of the Kairos Power gFHR, in which verification of the method was performed through code-to-code verification with the Kairos Power toolbox (Kile et al., 2022; Satvat et al., 2021).

1.3 Temperature Sensitivity of PB-HTGRs

In graphite moderated systems, like PB-HTGRs, there is a strong coupling between reactivity and temperature, largely due to the impact of temperature on the cross-sections of both the fuel and the graphite. Skutnik et. al. (Skutnik & Wieselquist, 2021) investigated the temperature effects on one-group cross-sections in the PBMR-400. This study found that temperature is a first-order consideration for cross-sections in PB-HTGRs because the location and shape of the thermal peak of the neutron spectrum is a strong function of the temperature of the fuel and the reflector. This shifting of the thermal peak as the result of increasing temperature led to the hardening of the neutron spectra and the shift of the flux closer to the absorption resonances of Pu-239, Pu-240 and U-238. In contrast, Doppler broadening showed only a small impact on the cross sections. Both the observed spectral shift and Doppler broadening illustrate the sensitivity of PB-HTGRs systems to temperature.

1.4 Scope of This Work

The goal of this work was to develop an equilibrium core model of a modular high-temperature gas-cooled reactor (mHTGR) similar to the Xe-100 using the SLICE method to assess the impact of temperature on the generation of the equilibrium fuel compositions. The first part of this study confirms the applicability of the generated equilibrium model by comparing the eigenvalue $k_{effective}$ and nuclide inventory of the SCALE equilibrium model to results generated by VSOP-A (Mulder & Boyes, 2020) and the MEEES-PBR (Lu & Wu, 2022). Afterwards, the impact of temperature on the eigenvalue $k_{effective}$ and the nuclide inventory at equilibrium is assessed by investigating the discharge nuclide inventory and $k_{effective}$ for three equilibrium models that were created with three different temperature profiles.

For reasons of completeness, it is mentioned that a recently published ORNL report also used the SLICE method to develop an Xe-100 type reactor model for purposes of fuel cycle analysis (Davidson et al., 2023). However, the model presented in this ORNL report was developed independently from the study presented here and it included several simplifications such as not modeling the lower cone. In contrast, the developed model here includes higher fidelity, and it is used for additional temperature related studies as described above, with the prospect of use in additional sensitivity studies in the future.

2. Methodology

2.1 Computational Modeling in SCALE

SCALE is a modeling and simulation suite that comprises an integrated framework of computational modules with various applications, including reactor physics and criticality safety

(Wieselquist & Lefebvre, 2023). The SCALE modules used for the SLICE method were TRITON, ORIGEN, and ARP. TRITON is a reactor physics sequence that couples neutron transport calculations, here with the MC code KENO-VI, with depletion and decay calculations through ORIGEN to automate depletion calculations of detailed 3D models. For multigroup (MG) calculations, such as those used in this work, TRITON invokes the XSProc module for cross-section processing. An important role in the equilibrium modeling method is held by ORIGEN cross section libraries which are generated by TRITON. These are binary files containing burnup-dependent cross-sections and transition matrices that can be used by ORIGEN for standalone depletion and decay calculations. The ARP module can be used to interpolate the data on the libraries according to burnup, moderator density, and enrichment. Both TRITON and ORIGEN generate a burnup-dependent binary concentrations file that contains detailed nuclide inventories for more than 2,000 individually tracked nuclides and that can be viewed and manipulated with command-line tool OBIWAN.

A development version of SCALE 7.0, along with the latest SCALE 6.3.1 release (Wieselquist & Lefebvre, 2023), was employed for this work, using a 252-group cross section library based on the ENDF/B-VII.1 evaluated nuclear data library (Chadwick et al., 2011). SCALE 6.3.1 contains a unique method of treating doubly heterogenous (double-het) fuel in MG transport calculations (Skutnik & Wieselquist, 2021; Wieselquist & Lefebvre, 2023). The double-het nature of the fuel in the mHTGR arises from the heterogenous lattice of the fuel pebbles within the reactor combined with the heterogenous mixture of the TRISO particles in the graphite matrix within the fuel pebbles (Williams et al., 2015). As a result of the double-het treatment used in SCALE, it is not necessary to explicitly place the TRISO particles within the graphite matrix within the pebbles MG neutron transport calculations (Bostelmann et al., 2020; Ilas et al., 2012), like the SCALE model shown in Figure 1a. Instead, a double-het fuel mixture is created and used in the fuel region, shown in Figure 1b, dramatically reducing computation time compared to calculations with fully explicit models. All MC calculations in this work are performed with this double-het treatment. The specifications of the pebble geometry are listed in Table 1.

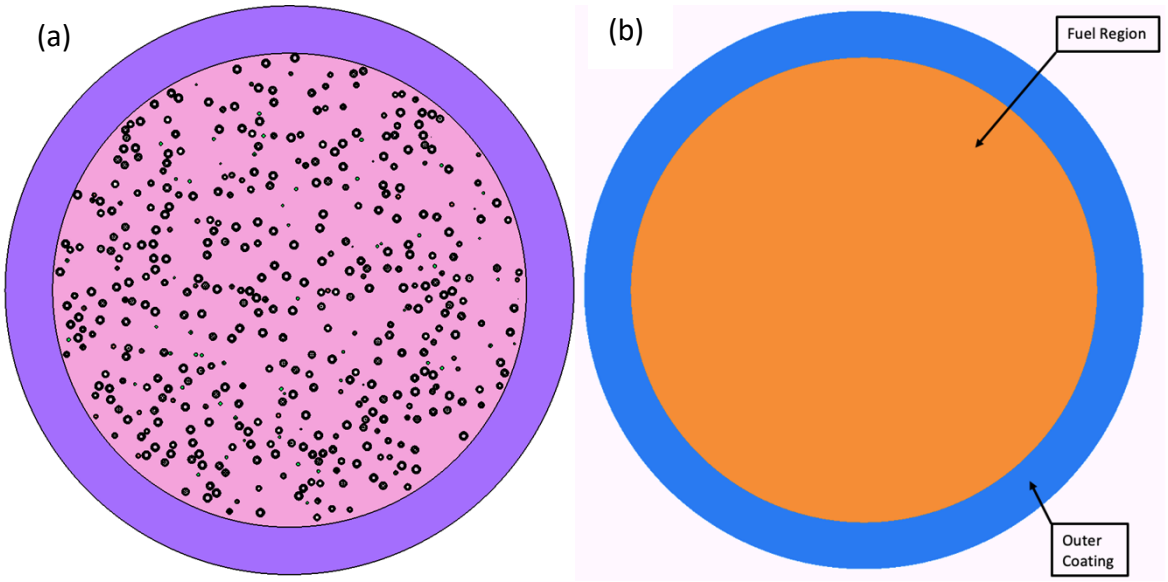

Figure 1. (a) SCALE model of a single mHTGR pebble with explicit TRISO placement (left). (b) SCALE MG model of a single mHTGR pebble (right).

Table 1. TRISO particle and fuel pebble parameters (Mulder & Boyes, 2020).

Parameter	Value
Fuel Type	UCO
Enrichment	15.5 wt% U-235
Uranium Loading per Pebble	7 g
Pebble Diameter	60 mm
Outer Coating Thickness	5 mm
TRISO Kernel Diameter	0.425 mm
# TRISO Particles per Pebble	19,542
UCO density	10.4 g/cm^3
Coating Materials	C/PyC/SiC/PyC
Layer Thicknesses	100/40/35/40 μm
Layer Density	1.05/1.9/3.2/1.9 g/cm^3

2.2 Development of SCALE Models

The SLICE method requires the use of two different SCALE models, a full-core model and a slice model, both of which contain fuel pebbles utilizing the specifications above. The full-core model of the mHTGR similar to the Xe-100 is shown in Figure 2. The core was divided into ten axial zones, which divide the active core height of 8.93 m into equal volume zones. Fuel zone 1 is located at the top of the core, and fuel zone 10 is at the bottom. Outside of the core are three layers of reflectors, which contain the reserve shutdown system (RSS) and the reactivity control system (RCS). Work published by Mulder and Boyes also indicates the presence of helium risers, but no specification of the number of risers is provided (Mulder & Boyes, 2020). As a

result, they were not included in the modeling. Within the full-core model, approximately 223,000 fuel pebbles are present (Mulder & Boyes, 2020). Pebble clipping is allowed in the core at the boundary of the reflector and at the boundaries between axial zones in order to simplify the modeling and to allow for defined boundaries between axial zones.

The second model that is used for the SLICE method is a slice model of the mHTGR, shown in Figure 3. As implied by the name, the slice model is simply an X-Y slice through the axial center of the mHTGR with axially reflective boundary conditions. The Z-dimension of the slice was chosen in a way that maintained the pebble packing with the reactor. Two types of pebbles were used within the slice model. The first pebble type used are the depletable surrogate pebbles, which are those that will be depleted during the TRITON calculations. These pebbles will have a fresh fuel composition at the beginning of every TRITON calculation. The second pebble type used are the non-depletable pebbles which are not depleted during the TRITON calculation. These pebbles are updated with the core-average composition at the end of each iteration. Within the slice, 10% of the pebbles are identified as surrogate pebbles and the remainder are non-depletable pebbles. The surrogate pebbles are spread out within the slice model to effectively capture the flux spectrum across the entire slice.

A dodecahedral lattice was used within both the slice and full-core model for the packing of the pebbles within the mHTGR core. The specifications for the lattice were such that the average pebble packing for the reactor, 5,394 pebbles per cubic meter, was maintained. Previous studies compared the use of an ordered hexagonal lattice to a randomly packed pebble bed in PBRs found a negligible difference between the two configurations (Kile et al., 2022; Skutnik & Wieselquist, 2021). Table 2 lists the geometry and material specifications used to build the full-core and slice models. These specifications are for a 165 MW_{th} version of the Xe-100 (Mulder & Boyes, 2020), rather than the 200 MW_{th} design that X-Energy plans to deploy commercially. The specifications of the 165 MW_{th} reactor were utilized in order to compare the results to other previously published work (Lu & Wu, 2022; Mulder & Boyes, 2020).

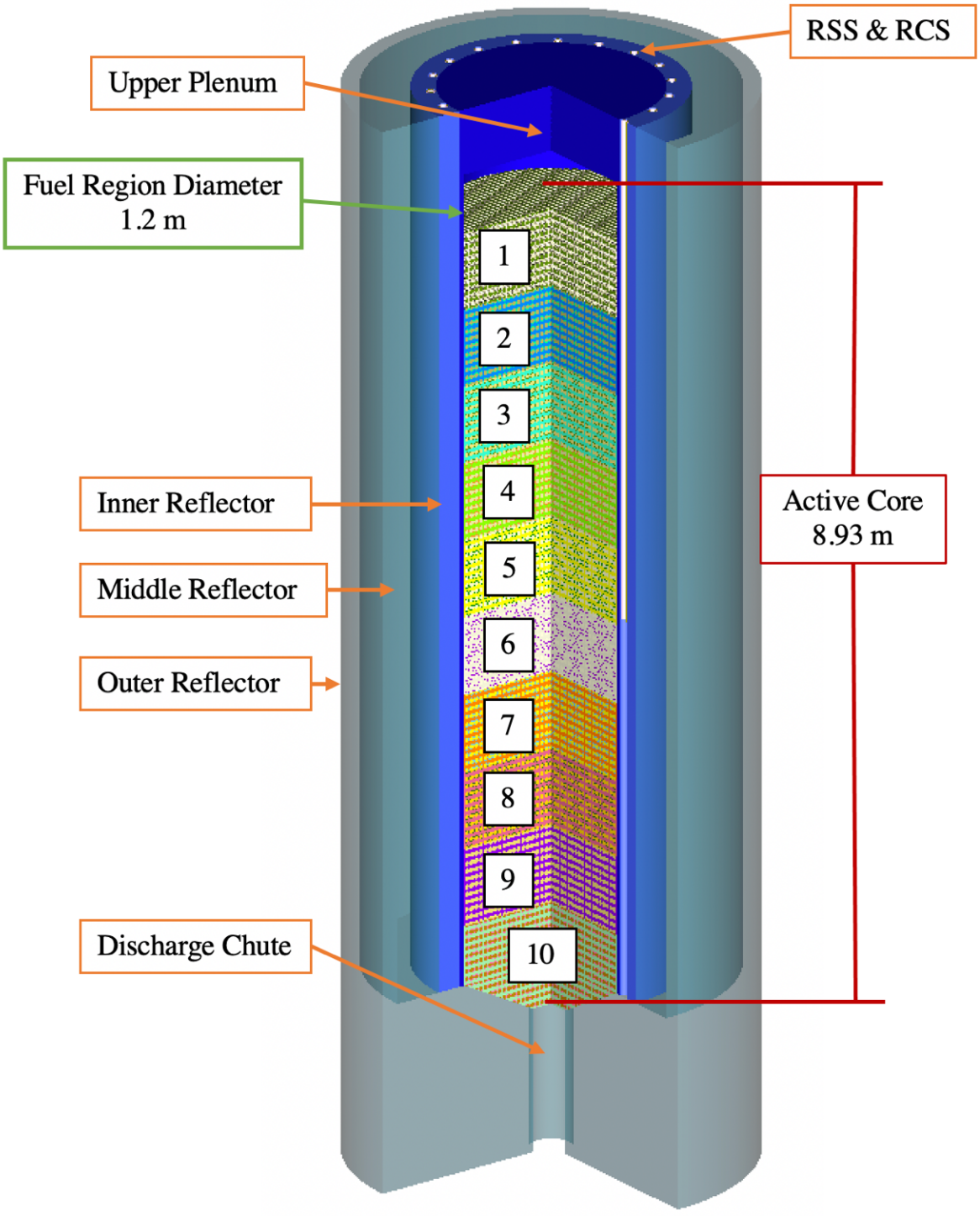

Figure 2. SCALE Full-core model of a mHTGR similar to the Xe-100.

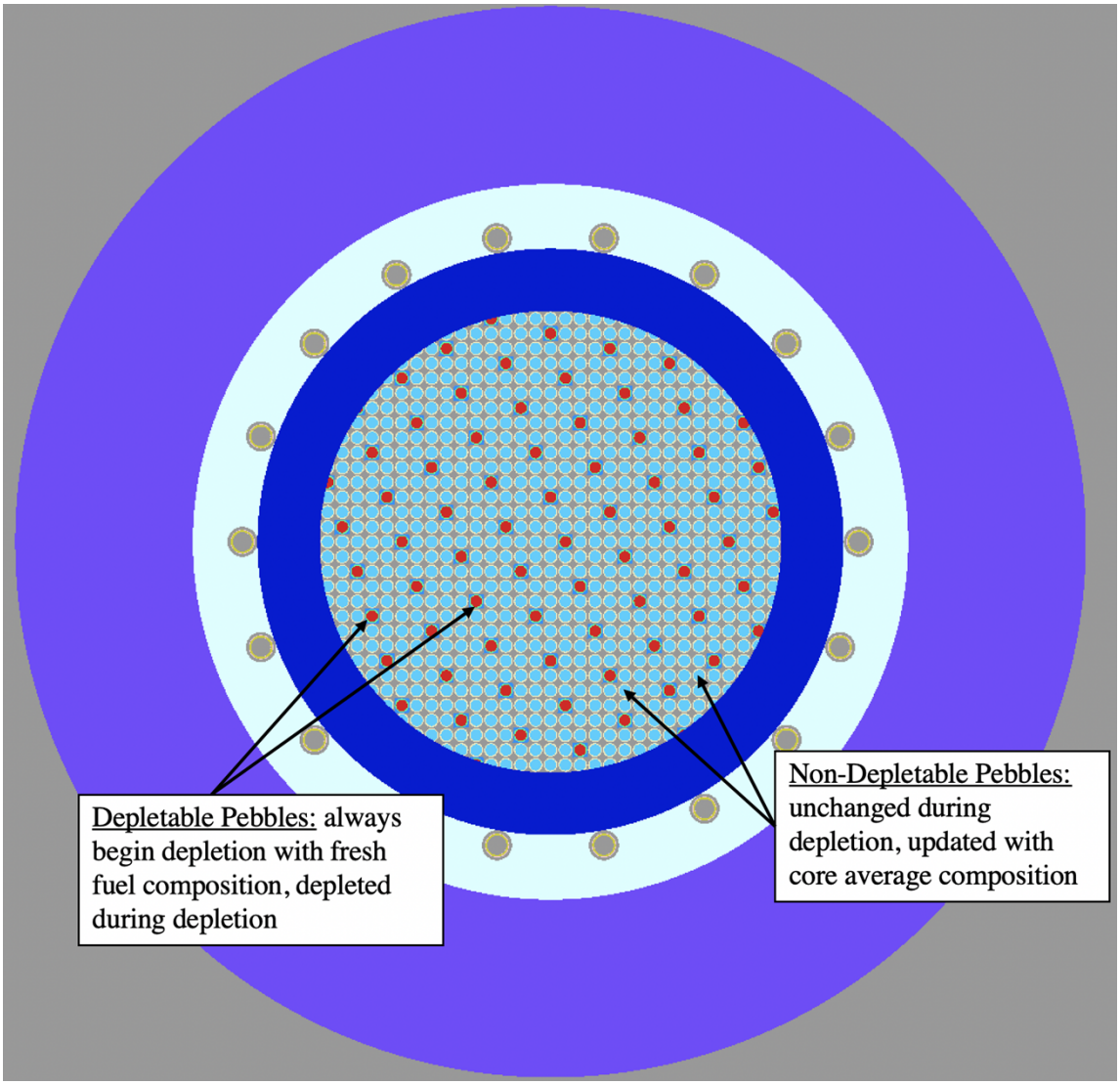

Figure 3. Slice model of the mHTGR similar to the Xe-100.

Table 2. mHTGR core parameters and dimensions (Lu & Wu, 2022; Mulder & Boyes, 2020).

Parameter	**Value**
Core Radius	1.20 m
Core Height	8.93 m
Thermal Power Rating	165 MW
Average Burnup	165,000 MWd/t_{HM}
Average Core Power Density	3.99 MW/m^3
Pebble Bed Packing	5,394 pebbles/m^3
Pebbles in Core	~223,000 pebbles
Fuel/TRISO Layers and Bulk Graphite Temperature	900/600 K
Cycle Length	1,549 EFPD

Number of Passes	6 passes

2.3 SLICE method

The SLICE method is shown in Figure 4. The method is comprised of two different iterations. The purpose of the inner iterations is to converge upon zone-average fuel inventories (assuming a specific power, target burnup, and an axial power profile), which are then used in the full-core MC calculation to get an updated axial full-core power profile (outer iteration). The very first inner iteration begins with all the pebbles within the slice model, surrogate and non-depletable, having a fresh fuel composition. Then a TRITON depletion calculation is performed, only depleting the surrogate pebbles while the compositions in the non-depletable fuel pebbles remain unchanged during depletion. As listed in Table 2, the pebbles in the mHTGR are expected to pass through the core 6 times during each cycle. To account for this, six depletion sub-intervals, representing the six passes that a pebble will make through the core, are used in the depletion calculation within TRITON. Besides burnup-dependent fuel compositions and $k_{effective}$, the TRITON calculation results in the generation of a burnup-dependent ORIGEN cross-section library that contains one-group cross sections at the middle of each pass. After interpolating these one-group cross sections with ARP to the desired burnups, they are used in ORIGEN power depletion calculations to determine burnup-dependent nuclide inventories for *each pass and zone*. The power used with ARP and ORIGEN is thereby determined from the burnup-dependent specific power of a pebble during depletion and the relative full-core power profile to correctly consider the different power levels in the different axial zones of the core. The compositions are blended together with OBIWAN to generate zone-average and core-average compositions. For the first pass through the inner iterations, there is no previous iteration to compare to in order to determine if convergence has occurred, so the next inner iteration begins. For the second inner iteration, the fuel composition of the non-depletable pebbles is updated with the core-average composition that was found during the first inner iteration. However, the surrogate pebbles retain the fresh fuel composition. The depletion time is also updated to match the desired discharge burnup. While the matching of the discharge burnup to the target burnup was chosen as a condition for this work, targeting a cycle length could be a potential alternative boundary condition.

The second inner iteration moves through the same steps as previously described until the end of the iteration. At the end of the second inner iteration, the metrics of convergence are compared between the first and second iteration. These metrics are listed in Table 3. If convergence has not occurred, the depletion time and surrogate pebble compositions are updated, and the next inner iteration begins. The inner iterations continue until the convergence criteria have been met. Once this occurs, the method moves to the outer iteration. During this outer iteration, the zone-average fuel compositions that were generated by the most recent inner iteration are used to populate the fuel compositions of the respective axial zones of the full-core model. Then a single neutron transport calculation of the full-core model is performed with TRITON in order to obtain the flux and relative power in each of the axial zones. The relative powers in each axial zone are used to construct an axial relative power profile. Starting again with the inner iterations, the first inner iteration begins again with a fresh fuel composition in both the surrogate and non-depletable pebbles. The inner iterations progress as described above, with the only difference being the relative power profile that is applied to the ARP and ORIGEN calculations. For the first outer iteration, the relative power profile is unknown, so a constant

value of one was used for all axial zones. For the second outer iteration, the relative power profile is updated with the relative power profile found during the previous outer iteration. This iterative method continues until there is convergence of the power profile. Once convergence of the relative full-core power profiles occur, equilibrium has been found.

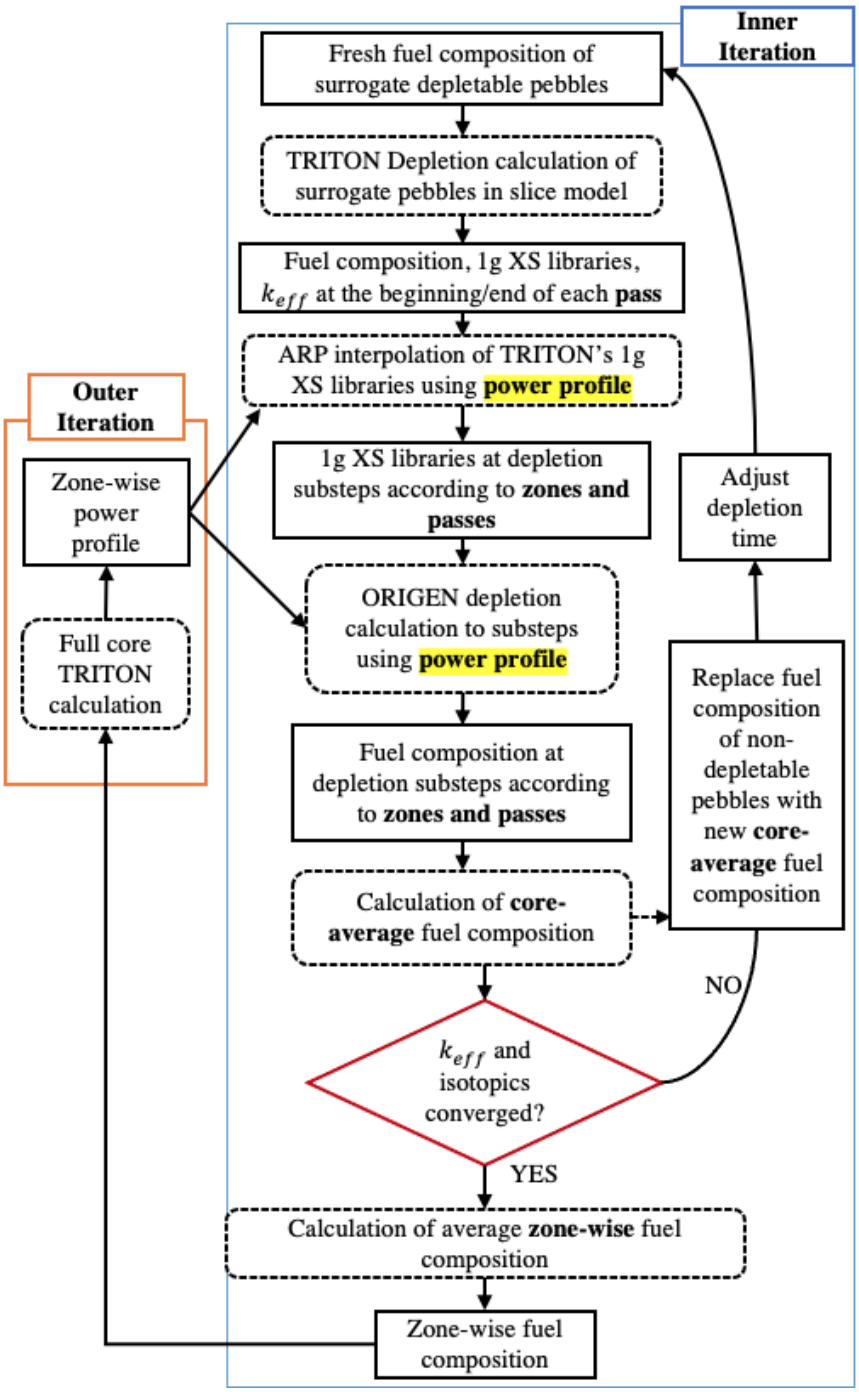

Figure 4. SLICE method.

Table 3. Convergence metrics used for inner iteration convergence determination (Kile et. al, 2022).

Metric	**Convergence Criteria**
$k_{effective}$ value	Within 20 percent millirho (pcm) of the previous iteration
Nuclide Concentration (at/b-cm)	Within 0.5% of the previous iteration
Burnup (GWd/t_{HM})	Within 0.05% of the target burnup of 165 GWd/t_{HM}

2.4 Temperature Sensitivity Study

In order to determine the sensitivity of the equilibrium core results to the temperature, several different combinations of graphite and fuel temperatures were tested with the SLICE method. The same equilibrium modeling method and models as described above were used, with the only change being the fuel and non-fuel component temperatures. The temperature profiles used for the temperature sensitivity testing, temperature profile one and two, are listed alongside temperature profile three, which was used for the primary equilibrium modeling work, in Table 4. The temperatures in temperature profile one were taken from Lu and Wu (Lu & Wu, 2022), that lists temperatures of 900K and 600K for the fuel and non-fuel materials, respectively. The second temperature profile that was used was 1088.15K and 1068.15K as the fuel and non-fuel temperatures in the pebble, and 600K for the reflector. This fuel temperature was based on the average fuel temperature of 815℃ published by Mulder and Boyes (Mulder & Boyes, 2020). The provided fuel temperature, along with the expected temperature drop from the center of the TRISO particle to the matrix of 20 K (Ghezzi et al., 2022), were used to select the non-fuel pebble temperature. Because no specific information regarding the reflector temperature was provided, it remained at 600K. The temperature profile used for this work, temperature profile three, with 900K for the fuel pebble and 600K for the reflector, was chosen because it largely matched the profile used for the MEEES-PBR method, allowing a comparison between two methods that do not utilize thermal-hydraulic feedback. However, temperature profile three included a more reasonable representation of the temperature drop between the center of the fuel particle and the graphite matrix material resulting in a pebble temperature closer to the average temperature of 1088.15K published by Mulder and Boyes (Mulder & Boyes, 2020).

Table 4. Temperature profiles used for testing the temperature sensitivity of the equilibrium core.

	Fuel Temperature [K]	**Pebble Graphite and TRISO layer Temperature [K]**	**Reflector Temperature [K]**
Temperature Profile 1	900	600	600
Temperature Profile 2	1088.15	1068.15	600
Temperature Profile 3	900	900	600

3. Results

3.1 Approach to equilibrium results

Using the SLICE method described above for mHTGR, three outer iterations were needed to reach convergence, with an average of nine inner iterations needed within each outer iteration. The results shown in this section detail how the SLICE method converged upon the equilibrium core. Figure 5 shows the evolution of $k_{effective}$ over the inner iterations. Because the first inner iteration of all three outer iterations began with a fully fresh fuel slice, all three outer iterations had the same $k_{effective}$ value for iteration 0. The initial $k_{effective}$ of the slice model for each 0^{th} inner iteration was 1.35713 ± 0.00029. This exhibits the excess reactivity that would exist in an entirely fresh fuel core, which would not occur at any point in the lifetime of the mHTGR. This value is comparable to the one found by Lu and Wu (Lu & Wu, 2022).

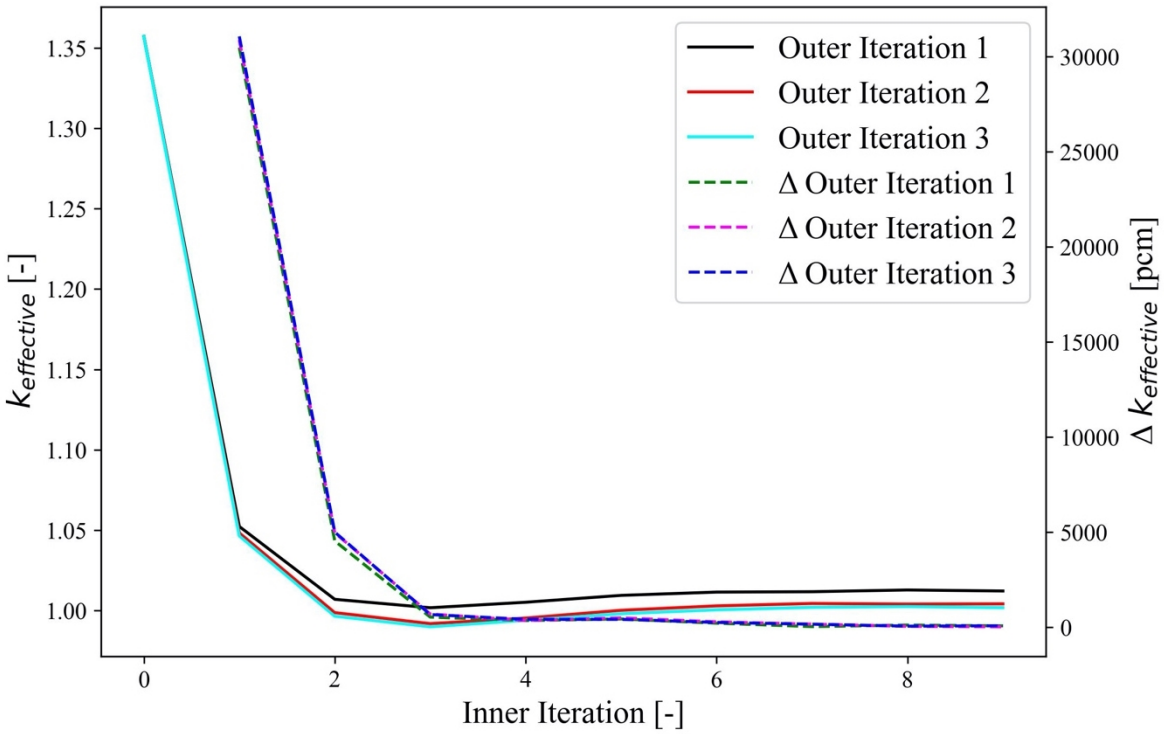

Figure 5. Evolution of $k_{effective}$ over the inner iterations for each outer iteration along with the $k_{effective}$ difference between the individual iterations.

The steep drop in $k_{effective}$ seen after the 0th iteration for all the outer iterations was the result of the updating of the non-depletable pebble composition from fresh fuel to the core-average inventory resulting from the 0th inner iteration. Figure 6 shows the evolution of the burnup as it converged to equilibrium over the inner iterations. This graph illustrates the large jump in the burnup that occurred between the 0th and 1st iteration, from 128.15 GWd/tHM to around 180 GWd/tHM for all the outer iterations. After this initial increase in burnup between iterations, the burnup began to decrease, moving towards the specified target burnup. As with $k_{effective}$, the initial large increase in burnup between inner iteration zero and one was the result of updating the non-depletable pebble inventory. For iteration zero, the non-depletable pebble inventory used for the TRITON depletion calculation was a fresh fuel inventory. As described previously, this TRITON depletion calculation was followed by the ARP-ORIGEN sequence, which produced a core-average inventory. For inner iteration one, this core-average inventory replaced the fresh fuel inventory in the non-depletable pebbles, which led to the large difference between inner iteration zero and one. Throughout the entire equilibrium search process, the changes in $k_{effective}$ and burnup were the result of changes to the nuclide inventory of the non-depletable pebbles as convergence at equilibrium was approached. The core-average nuclide inventory changes in response to improvements to the spectral conditions experienced by the surrogate pebbles during the TRITON depletion calculations. The changes in the neutron spectrum experienced by the surrogate pebbles were the result of the updating of the non-depletable pebbles with the core-average inventories from the previous iteration. As convergence begins to occur, the changes to the core-average inventory became less between each iteration, resulting in the convergence behavior seen in Figure 5 and Figure 6.

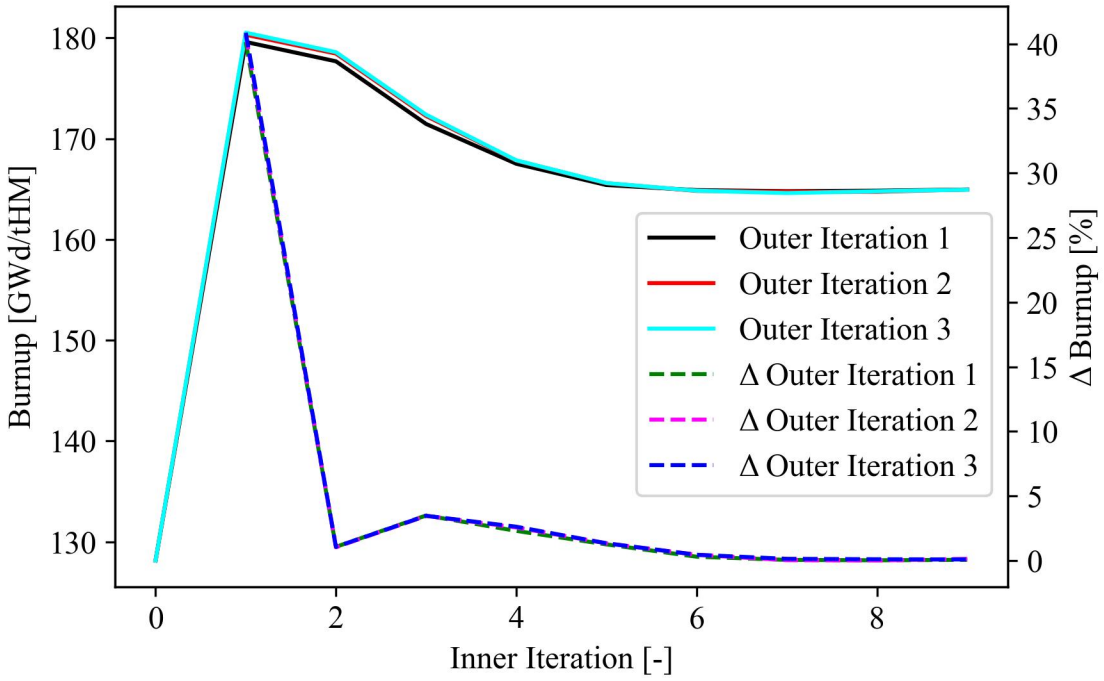

Figure 6. Evolution of burnup over the inner iterations for the three outer iterations and the percent change in burnup between the inner iterations.

Looking at the $k_{effective}$ evolution for the three outer iterations, the largest difference was between the first and second outer iterations. The reason why there was such a large change between these two outer iterations, but not between outer iteration two and three, was the relative power profile that was being applied to the ARP and ORIGEN calculations. As previously mentioned, for the first inner iteration a constant power profile was used for the ARP-ORIGEN calculation sequence, while relative power profiles from the full-core calculations were used in the second and third outer iterations. The power profiles that were used in outer iterations two and three were similar and therefore led to very similar results between these iterations. A comparison of the relative power profiles for the three outer iterations is shown in Figure 7. The relative power profiles resulting from outer iterations 1 and 2 showed differences in all zones, with a maximum difference of 11.05%. In contrast, the power profiles resulting from outer iterations 2 and 3 agreed well with a maximum difference of 4.80%. Therefore, it was determined that convergence had occurred with outer iteration 3.

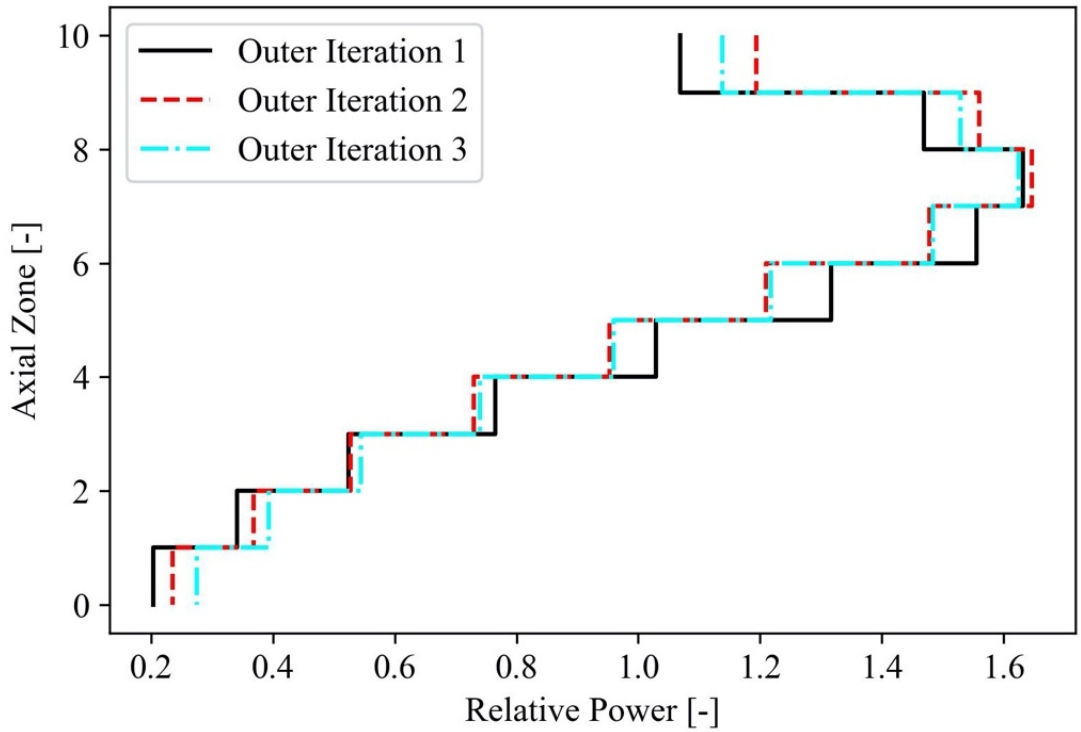

Figure 7. Relative power in each axial zone of the mHTGR similar to the Xe-100 for the three outer iterations.

Figure 8, Figure 9 and Figure 10 show the change in the core-average concentrations of U-235, U-238, and Pu-239 during the approach to equilibrium. The steep drop in the U-235 that occurred after the 0^{th} iteration was directly responsible for the similar drop that occurs in $k_{effective}$. This was the result of the update of the non-depletable pebble inventory from the initial fresh fuel inventory in iteration zero to the core-average inventory resulting from iteration zero for iteration one, as discussed above. The convergence of the core-average nuclide inventories was clearly reached after nine inner iterations for all three outer iterations.

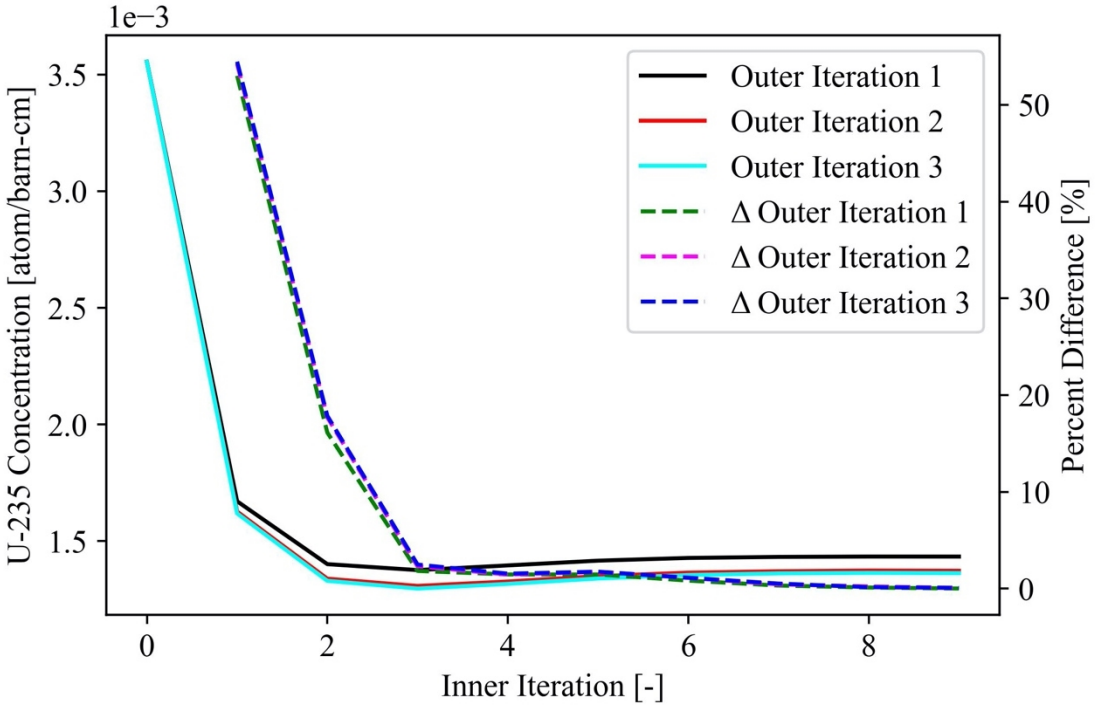

Figure 8. Evolution of the U-235 concentration over the inner iterations for the three outer iterations and the change in concentration between inner iterations.

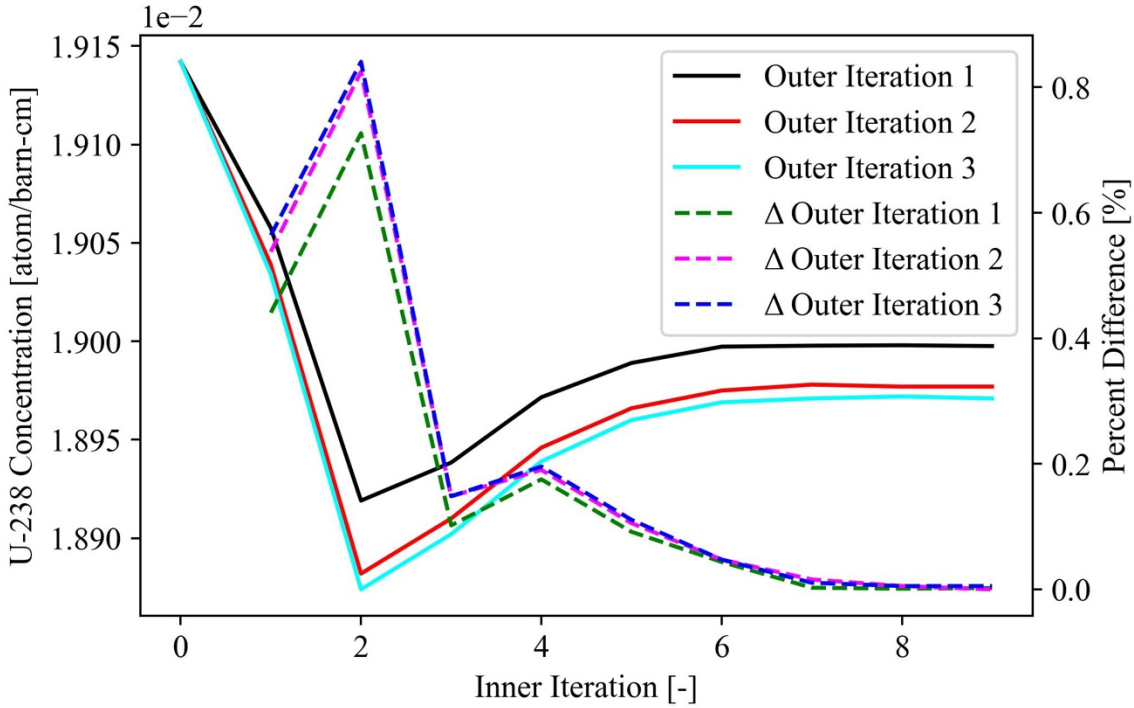

Figure 9. Evolution of the U-238 concentration over the inner iterations for the three outer iterations and the change in concentration between inner iterations.

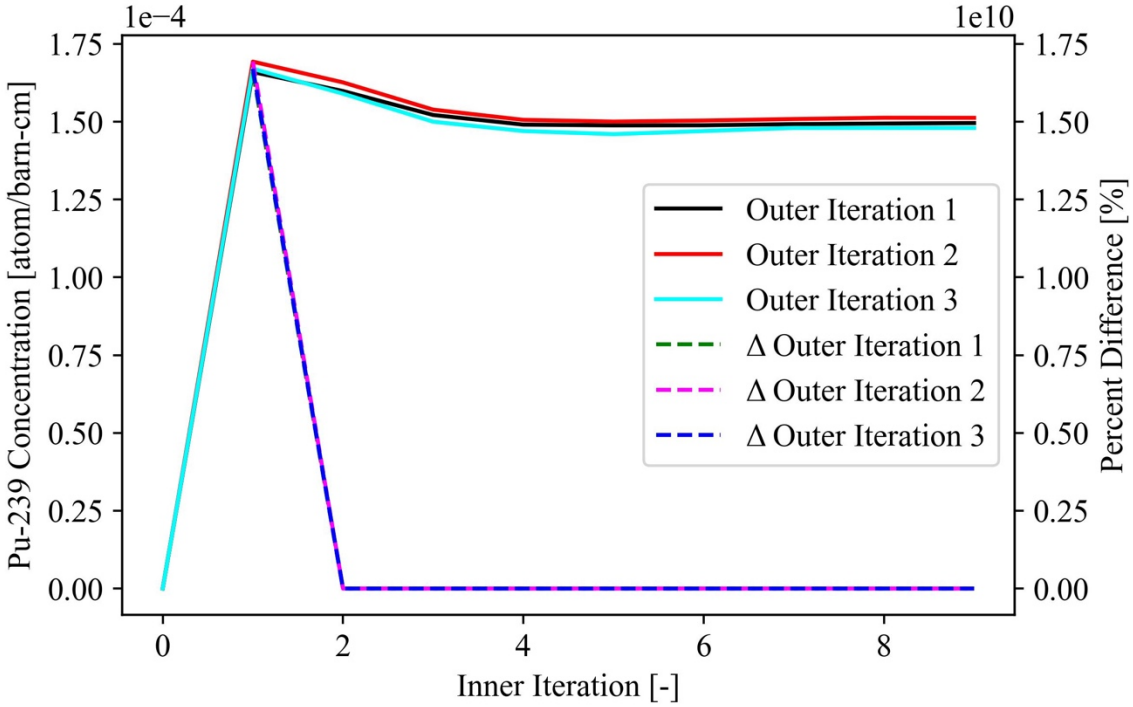

Figure 10. Evolution of the Pu-239 concentration over the inner iterations for the three outer iterations and the change in concentration between inner iterations.

3.2 Equilibrium Results

After convergence of the power profiles was determined at the conclusion of outer iteration three, the zone-average nuclide inventories were used to construct a full-core model of the mHTGR at equilibrium. The axial power profile and zone-average burnup of the full-core equilibrium model are shown in Figure 11. In the graph on the right of Figure 11, the zone-average burnup increases uniformly axially across the entirety of the core. This uniform increase is reflective of the assumption that the burnup of a pebble will increase uniformly as it passes through the reactor, from the top of the core to the bottom. The axial power profile of the full-core equilibrium model is shown in Figure 11 on the left. As expected, the peak power occurs in the upper zones of the reactor. This is due to the fact that the fuel enters at the top of the reactor, therefore at the top of the reactor the fuel is less burnt and consequently has more power at equilibrium.

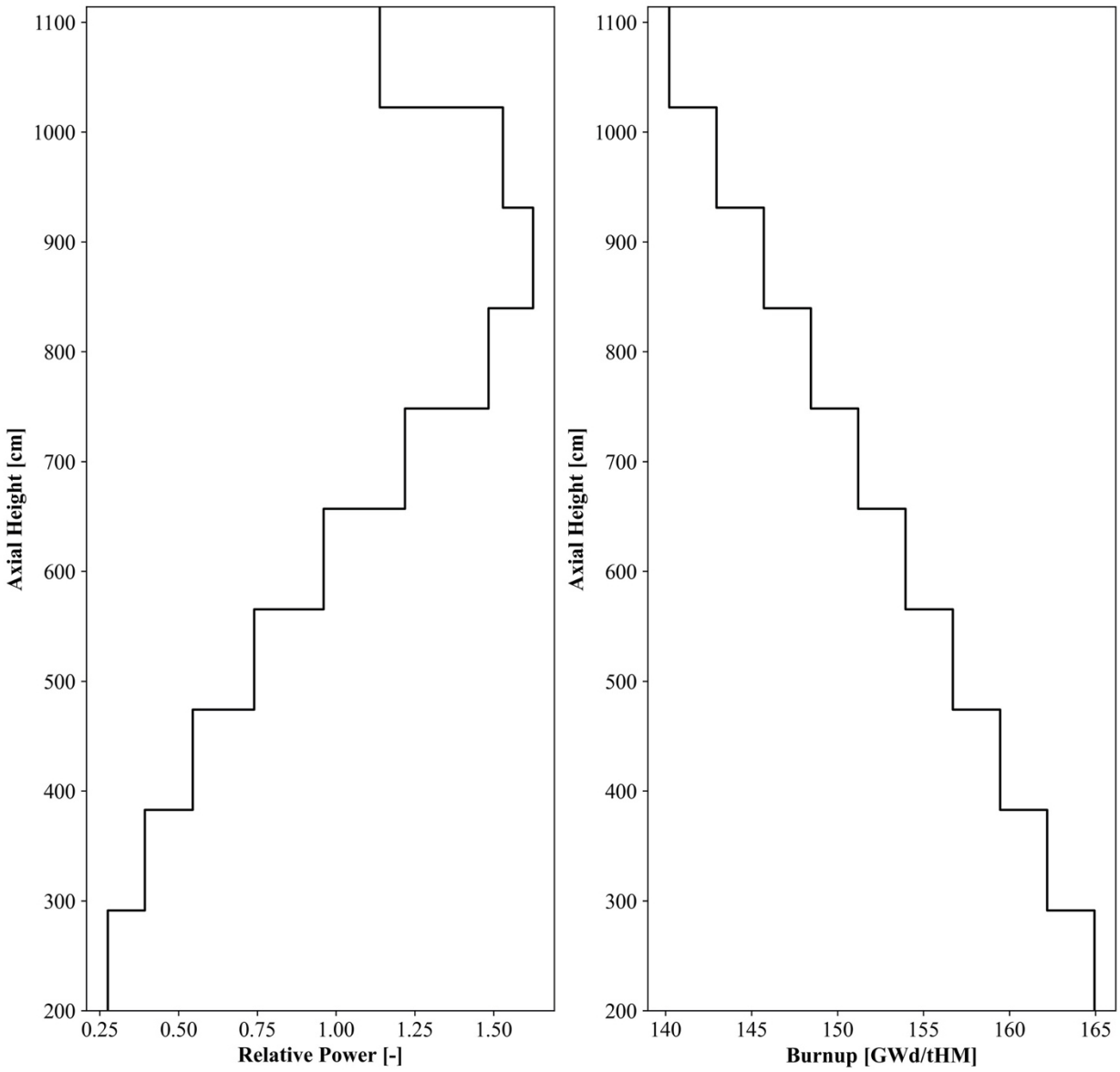

Figure 11. Relative power versus axial height for the full-core equilibrium model (left). Zone-average burnup versus axial height for the full-core equilibrium model (right).

The normalized flux profile across the reactor was compared to the profile published by Mulder and Boyes in Figure 12 (Mulder & Boyes, 2022). The SCALE results show the normalized thermal flux in each axial zone of the reactor. Both the magnitude of the normalized thermal flux, and the peak thermal flux location agree well between the SCALE and VSOP-A results (Mulder & Boyes, 2020). The width of the peak from the SCALE is slightly larger than that of the VSOP-A results, which can potentially be attributed to the use of zone-wise thermal fluxes for the SCALE flux profile. The most visible differences between the SCALE and VSOP-A results are the top of the reactor. The VSOP-A profile shows a significant decrease in thermal flux when moving upwards in the reactor from the location of the peak flux, with the flux at the top of the pebble-bed being approximately 20% of its value at the peak (Mulder & Boyes, 2020). The SCALE results show a less significant decrease, with the flux at the top of the pebble-bed

still being 60% of the peak value. This, again, can likely be attributed to the use of zonal fluxes, instead of discrepancies between the models, because the zonal fluxes are not as proficient in capturing the non-linear decrease in thermal flux within a zone.

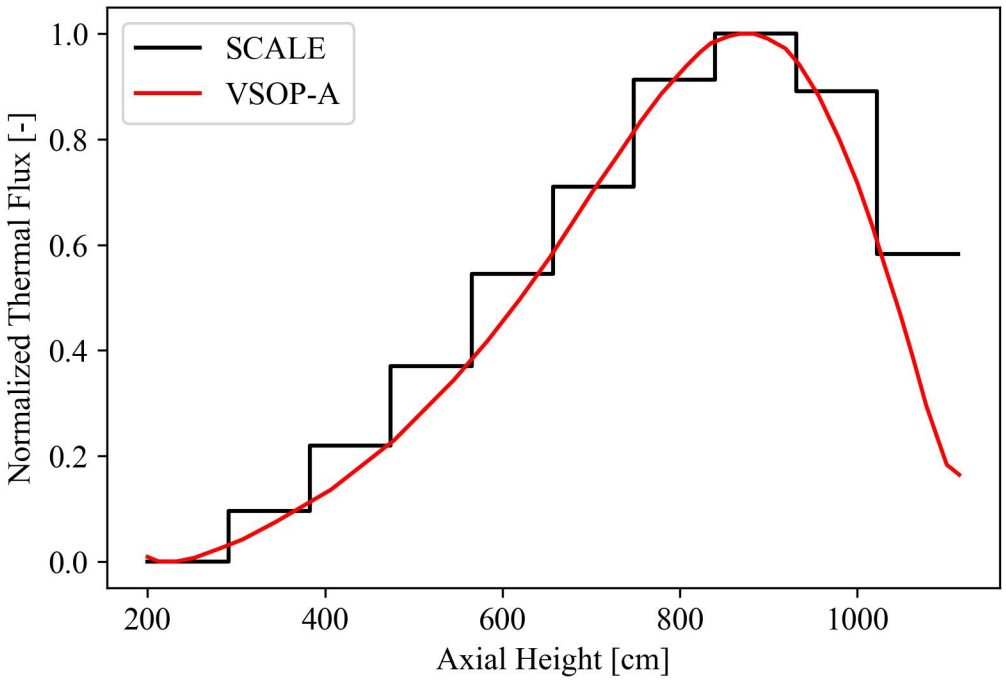

Figure 12. Comparison of the thermal flux at equilibrium between the SCALE and VSOP-A (Mulder & Boyes, 2020) results.

The equilibrium $k_{effective}$ value of the final full-core model was found to be 1.00862 $\pm$ 0.00023. This value is compared to the equilibrium $k_{effective}$ results found using the MEEES-PBR method and VSOP-A in Table 5 (Lu & Wu, 2022; Mulder & Boyes, 2020). There were differences between the equilibrium $k_{effective}$ values found using VSOP-A and the MEEES-PBR and the full-core equilibrium $k_{effective}$ found using the SLICE method. Some of the differences between the methods may be attributed to differences in calculation methods, which have been discussed in previous sections. Another source of differences could be the assumptions that are made using the SLICE method, such as using a limited number of depletable pebbles to capture the spectral effects, utilizing a reflective boundary slice model for the transport and depletion calculations, or targeting a burnup rather than a pebble residence time. However, the difference between the results from SCALE and the other results is significant enough that other sources of the error outside the equilibrium modeling method must be considered. Assuming that the geometry of the different models and the non-fuel compositions are similar, a remaining potential cause of differences in the $k_{effective}$ values between methods is the temperature chosen for the different components of the model.

Table 5. Comparison of the equilibrium $k_{effective}$ values between the full-core SCALE equilibrium model, MEEES-PBR (VCU), and VSOP-A (X-Energy) results.

	$k_{effective}$	Δk [pcm]
SCALE	1.00862 +/- 0.00023	(ref)
MEEES-PBR (Lu & Wu, 2022)	1.00233	629 $\pm$ 23
VSOP-A (Mulder & Boyes, 2020)	1.0015	712 $\pm$ 23

3.3 Sensitivity of the Equilibrium Core to Component Temperature

The equilibrium $k_{effective}$ comparison in the previous section illustrated the difference between the equilibrium $k_{effective}$ found using the SLICE method and the VSOP-A equilibrium $k_{effective}$. As mentioned, while there are several reasons for the difference, the absence of thermal-hydraulic feedback in the SLICE method is expected to be the main contributor to the difference, due to the strong coupling of temperature to reactivity in graphite moderated systems. In addition to the temperature profile used for the original equilibrium modeling, two additional temperature profiles, shown in Table 4, were used to generate equilibrium cores. The resulting full-core $k_{effective}$ values at equilibrium for the three temperature profiles are compared in Table 6 to the VSOP-A results.

Table 6. Calculated mHTGR full-core equilibrium $k_{effective}$ values for three temperature profiles.

	Equilibrium $k_{effective}$	Δk [pcm]
VSOP-A (Mulder & Boyes, 2020)	1.0015	(ref)
Temperature Profile 1	1.01371 $\pm$ 0.00033	1,221 $\pm$ 33
Temperature Profile 2	1.00530 $\pm$ 0.00025	380 $\pm$ 25
Temperature Profile 3	1.00862 $\pm$ 0.00023	712 $\pm$ 23

Comparing the equilibrium $k_{effective}$ values to the VSOP-A equilibrium $k_{effective}$ of 1.0015 (Mulder & Boyes, 2020), temperature profile 1 resulted in an overprediction of $k_{effective}$ by 1,221 pcm and temperature profile 2 resulted in an overprediction of 380 pcm. The best performing temperature profile relative to the VSOP-A results was temperature profile 2, which was built off the core average temperature provided in the reports. The eigenvalue differences up to 1,221 pcm between the models with different temperature profiles stresses the impact of temperature on the neutronics parameters. To better understand how the depletion calculations are impacted by differing temperature profiles, the discharge isotopics of the three models with the different temperature profiles are shown in Figure 13. The isotopes of interest were selected as they are both important to the reactivity of the reactor, but also undergo doppler broadening. As seen in the graphs in the upper and lower right of Figure 13, there is very little difference in the U-238 and Pu-240 concentrations at discharge between the three temperature profiles. However, there are more differences between the temperature profiles for the U-235 and Pu-239 concentrations at discharge. The U-235 and Pu-239 concentrations of temperature profiles one and two are compared in Table 7 to the discharge concentrations of temperature profile three, which serves as a reference value.

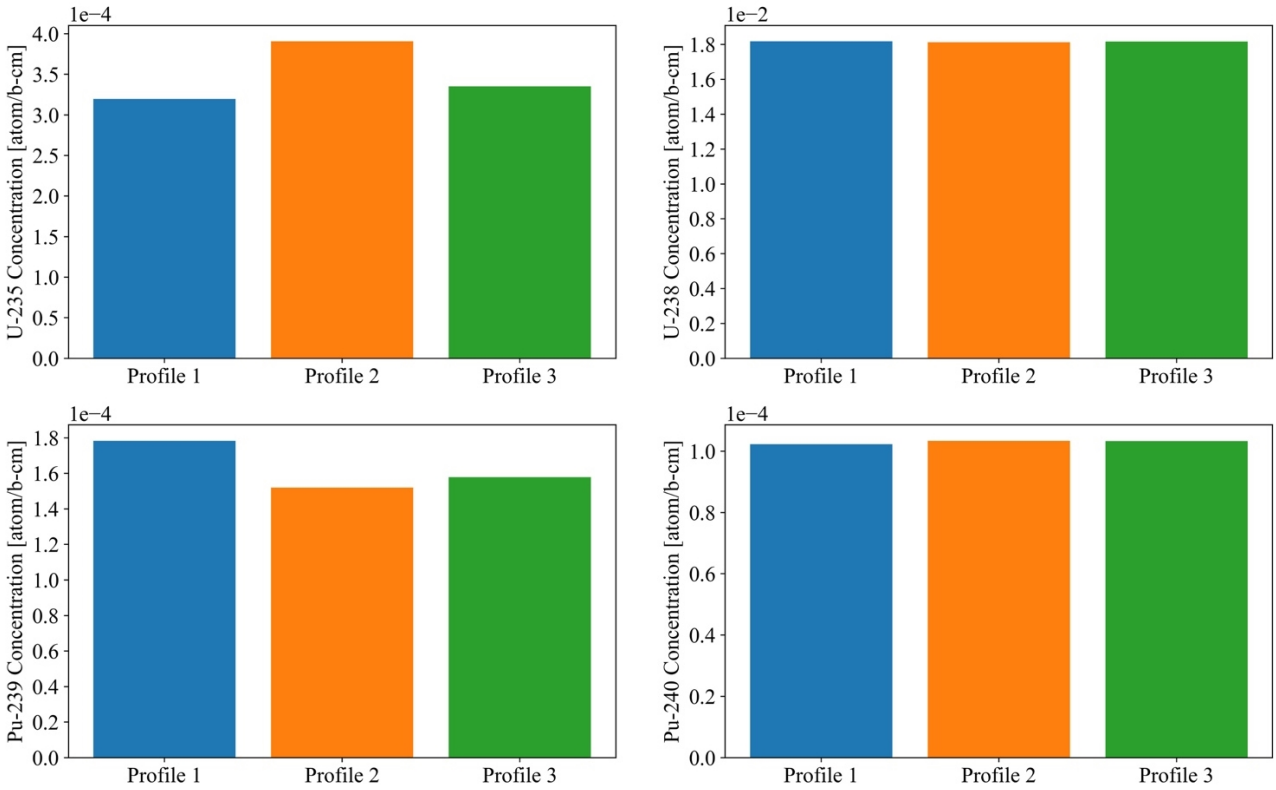

Figure 13. Comparison of discharge nuclide inventories between the different temperature profiles for U-235 (upper left), U-238 (upper right), Pu-239 (lower left), and Pu-240 (lower right).

Table 7. Differences in discharge concentrations between temperature profiles one and two to the reference temperature profile.

Temperature Profile	U-235 Difference from Reference [%]	Pu-239 Difference from Reference [%]
Temperature Profile 1	-4.78%	12.22%
Temperature Profile 2	15.25%	-3.79%
Temperature Profile 3	(ref)	(ref)

The impact of the temperature on the equilibrium core is clearly seen in the differences in the nuclide inventory at discharge between the different temperature profiles. The use of lower temperature of non-fuel materials, seen in the comparison of temperature profile 1 and 3, resulted in a 12.22% increase in the Pu-239 concentration at discharge. Using higher fuel and non-fuel material temperatures, seen in the comparison between temperature profile 2 and 3, resulted in a 15.25% increase in the discharge U-235. This increase in discharged fissile U-235 likely contributed to the lower full-core equilibrium $k_{effective}$ value found for temperature profile two compared to temperature profile three, shown in Table 6. The observed differences in the discharge inventory due to temperature would also impact the comparison between the SCALE equilibrium discharge inventory and VSOP's discharge inventory that is made in the next

section. The impact of detailed temperature profiles on equilibrium core generation should be studied next to obtain a better understanding of the sensitivity to temperature for inventory generation of the equilibrium core.

3.4 Nuclide Inventory Comparison

Mulder and Boyes published the mass-per-pebble of different plutonium isotopes after the 6th pass through the reactor for the purpose of providing a proliferation profile for the Xe-100 (Mulder & Boyes, 2020). While it was not explicitly stated, it was assumed that the provided mass distribution corresponds to a discharged pebble from an equilibrium core. The comparison of the discharge isotopics of the SLICE method and VSOP-A results are shown in Table 8. The difference between the plutonium inventory at equilibrium of the SLICE method compared to the inventory published by Mulder and Boyes (Mulder & Boyes, 2020) was between 2.32% and 9.51%. The best agreement was between the Pu-241 inventories, with the percent difference being only 2.32%. The largest disagreement was between the Pu-240 inventories, with a 9.51% difference. In addition to comparing the plutonium inventories at discharge, a comparison of U-235 inventories at the end of pass five was performed (Table 9). A larger difference in inventory is observed when comparing the U-235 inventory, with the SCALE U-235 inventory being 38.4% higher at the end of pass five than that of VSOP-A. This difference, along with the difference in the Pu-239 inventory, aligns with the results found in the previous section. As seen in Figure 13, variations in the component temperatures had a large impact on the U-235 and Pu-239 discharge isotopics of the mHTGR. Interestingly, temperature profile 2, which was based on the average fuel temperature published by Mulder and Boyes (Mulder & Boyes, 2020), had a higher discharged U-235 inventory than the reference case, but produced a $k_{effective}$ closer to that of VSOP-A at equilibrium. Theses discrepancies are likely due to the use of thermal-hydraulic feedback in VSOP-A which cannot be fully replicated through the use of a representative temperature profile. However, the testing of the different temperature profiles still illustrates the importance of the consideration of temperature when modeling equilibrium cores.

Overall, the differences between both the plutonium and U-235 inventories can likely be attributed to the inclusion of thermal-hydraulic feedback. Additionally, there are differences in the nuclear data libraries used to produce the SCALE and VSOP-A results that may have contributed to the observed differences in inventories. Lu and Wu indicate that VSOP-A utilizes the ENDF/B-VII data library, but they do not provide the specific version (Lu & Wu, 2022). ENDF/B-VII.0 and ENDF/B-VII.1 include significant differences in key nuclear data, including cross-sections of the plutonium isotopes compared in Table 8 (Bostelmann et al., 2021). The previously discussed assumptions could also have impacted the discharge inventory, along with computational differences, such as the inclusion of control rod movement.

Table 8. Nuclide inventory comparison between VSOP-A and SCALE at discharge.

	Pu-239 mass/pebble [g]	**Pu-240 mass/pebble [g]**	**Pu-241 mass/pebble [g]**	**Pu-242 mass/pebble [g]**
SCALE	0.0492	0.0323	0.0223	0.0270
VSOP-A (Mulder & Boyes, 2020)	0.0523	0.0294	0.0226	0.0245

Δ mass/pebble [g]	-3.11×10^{-3}	2.94×10^{-3}	-5.19×10^{-4}	2.07×10^{-3}
Difference [%]	6.12	9.51	2.32	8.12

Table 9. U-235 inventory comparison between SCALE and VSOP-A (Mulder & Boyes, 2020) at the end of pass 5.

	U-235 mass/pebble [g]
SCALE	0.1538
VSOP-A (Mulder & Boyes, 2020)	0.1043
Δ mass/pebble [g]	0.0495
Difference [%]	38.4

4. Conclusions

This work applied ORNL's SLICE method to generate an equilibrium full-core model of an mHTGR similar to the Xe-100. This method utilizes an iterative process that is comprised of outer and inner iterations. The inner iterations utilize a 2D slice model and seek convergence of the region-wise inventories of the equilibrium core, while the outer iterations are used to update the applied power profile. After three outer iterations, convergence of the power profile was attained, and the equilibrium core was reached. The full-core equilibrium model had an equilibrium $k_{effective}$ of 1.00862 ± 0.00023, which differed from the VSOP-A (Mulder & Boyes, 2020) and MEEES-PBR (Lu & Wu, 2022) results by 712 and 629 pcm, respectively. It is notable that the eigenvalue uncertainty due to uncertainties in nuclear data alone in an HTGR is at least 600 pcm (Bostelmann et al., 2020), without accounting for the impact of compounded uncertainties in burnup, geometry, and thermal feedback. The plutonium inventory at discharge showed a difference between SCALE and VSOP-A of 9.51% and 2.32% for Pu-240 and Pu-241, respectively. The U-235 inventories were compared after the 5th pass and shows a difference of 38.4%.

To better understand the difference between the full-core equilibrium $k_{effective}$ and discharge inventory found in this work compared to VSOP-A (Mulder & Boyes, 2020), which uses thermal-hydraulic feedback, a study was conducted to determine the sensitivity of the full-core equilibrium $k_{effective}$ and discharge inventory to the temperature profile used within the mHTGR. As anticipated, the generation of equilibrium inventory was found sensitive to the applied temperatures. The resulting full equilibrium core calculations provided $k_{effective}$ values with differences of several hundred pcm between the different models. Additionally, the nuclide inventory at discharge differed up to 15.25% between the temperature profiles. Given the uncertainties surrounding the parameters of the Xe-100 and the associated large differences between the modeling methods, the comparison of the SLICE method, along with the MEEES-PBR and VSOP-A, to a benchmark problem could offer resolution to some of the uncertainties identified in this work. A comparison of methods using a benchmark problem would allow for the understanding of how differences between the computational modeling methods impact the equilibrium results.

5. Acknowledgements

This material is based on work supported under an Integrated University Program Graduate Fellowship. Any opinions, findings, conclusions, or recommendations expressed in this publication are those of the authors and do not necessarily reflect the views of the US Department of Energy's Office of Nuclear Energy.

One author (N. R. Brown) was partially funded by a synergistic ARPA-E ONWARDS project called MATRICY.

6. References

Bäumer, R., Kalinowski, I., Röhler, E., Schöning, J., & Wachholz, W. (1990). Construction and operating experience with the 300-MW THTR nuclear power plant. *Nuclear Engineering and Design*, *121*(2), 155-166. https://doi.org/https://doi.org/10.1016/0029-5493(90)90100-C

Bostelmann, F., Celik, C., Williams, M. L., Ellis, R. J., Ilas, G., & Wieselquist, W. A. (2020). SCALE capabilities for high temperature gas-cooled reactor analysis. *Annals of Nuclear Energy*, *147*, 107673. https://doi.org/https://doi.org/10.1016/j.anucene.2020.107673

Bostelmann, F., Ilas, G., Celik, C., Holcomb, A. M., & Wieselquist, W. A. (2021). *Nuclear Data Assessment for Advanced Reactors*. https://www.osti.gov/biblio/1840202

Bostelmann, F., Celik, C., Kile, R. F. , and Wieselquist, R. F. , "SCALE Analysis of a Fluoride Salt-Cooled High-Temperature Reactor in Support of Severe Accident Analysis," ORNL/TM-2021/2273, Oak Ridge National Laboratory, Oak Ridge, TN, 2022. https://www.osti.gov/biblio/1854475

Chadwick, M. B., Herman, M., Obložinský, P., Dunn, M. E., Danon, Y., Kahler, A. C., Smith, D. L., Pritychenko, B., Arbanas, G., Arcilla, R., Brewer, R., Brown, D. A., Capote, R., Carlson, A. D., Cho, Y. S., Derrien, H., Guber, K., Hale, G. M., Hoblit, S., . . . Young, P. G. (2011). ENDF/B-VII.1 Nuclear Data for Science and Technology: Cross Sections, Covariances, Fission Product Yields and Decay Data. *Nuclear Data Sheets*, *112*(12), 2887-2996. https://doi.org/https://doi.org/10.1016/j.nds.2011.11.002

Davidson, E., Skutnik, S., Ritcher, Z., & Munk, M. (2023). *Modeling and Simulation of Xe-100type Pebble Bed Gas-Cooled Reactorwith SCALE*. https://www.osti.gov/biblio/1997735

https://www.osti.gov/servlets/purl/1997735

Dow, X-energy to drive carbon emissions reductions through deployment of advanced small modular nuclear power. (2022, August 9th, 2022). X-Energy. https://corporate.dow.com/en-us/news/press-releases/dow--x-energy-to-drive-carbon-emissions-reductions-through-deplo.html

Ghezzi, C. G., Kile, R. F., & Brown, N. R. (2022). TRISO SiC Failure Probability for Reactivity Initiated Accidents in High-Temperature Gas-Cooled Reactors. *Nuclear Science and Engineering*, *196*(11), 1361-1382. https://doi.org/https://doi.org/10.1080/00295639.2022.2097466

Ilas, G., Ilas, D., Kelly, R., & Davidson, E. E. (2012). Validation of SCALE for high temperature gas-cooled reactors analysis. (ORNL/TM-2011/161). https://www.osti.gov/biblio/1048709

Jian, F., Yingxue, J., Hongyong, C., & Wei, C. (2014). Overview and Progress of High Temperature Reactor Pebble-bed Module Demonstration Project (HTR-PM). 7th International Topical Meeting on High Temperature Reactor Technology, China.

Kadak, A. C. (2005). A future for nuclear energy: pebble bed reactors. *International journal of critical infrastructures*, *1*(4), 330-345. https://doi.org/https://doi.org/10.1504/IJCIS.2005.006679

Kile, R. F., Bostelmann, F., Skutnik, S. E., Wieselquist, W. A., & Brown, N. R. (2022). Assessment of SCALE and MELCOR for a generic pebble bed fluoride high-temperature reactor. *Annals of Nuclear Energy*, *173*, 109107. https://doi.org/https://doi.org/10.1016/j.anucene.2022.109107

Krüger, K., Ivens, G., & Kirch, N. (1988). Operational experience and safety experiments with the AVR power station. *Nuclear Engineering and Design*, *109*(1-2), 233-238. https://doi.org/https://doi.org/10.1016/0029-5493(88)90164-1

Leppänen, J. (2013). Serpent–a continuous-energy Monte Carlo reactor physics burnup calculation code. *VTT Technical Research Centre of Finland*, *4*, 455.

Lu, C., & Wu, Z. (2022). A New Method to Efficiently Estimate the Equilibrium State of Pebble Bed Reactors. *Nuclear Technology*, *208*(10), 1577-1590. https://doi.org/10.1080/00295450.2022.2049966

Mulder, E. J., & Boyes, W. A. (2020). Neutronics characteristics of a 165 MWth Xe-100 reactor. *Nuclear Engineering and Design*, *357*. https://doi.org/https://doi.org/10.1016/j.nucengdes.2019.110415

Satvat, N., Sarikurt, F., Johnson, K., Kolaja, I., Fratoni, M., Haugh, B., & Blandford, E. (2021). Neutronics, thermal-hydraulics, and multi-physics benchmark models for a generic pebble-bed fluoride-salt-cooled high temperature reactor (FHR). *Nuclear Engineering and Design*, *384*, 111461. https://doi.org/https://doi.org/10.1016/j.nucengdes.2021.111461

She, D., Chen, F., Xia, B., & Shi, L. (2021). Simulation of the HTR-10 operation history with the PANGU code. *Frontiers in Energy Research*, *9*, 704116. https://doi.org/https://doi.org/10.3389/fenrg.2021.704116

She, D., Guo, J., Liu, Z., & Shi, L. (2019). PANGU code for pebble-bed HTGR reactor physics and fuel cycle simulations. *Annals of Nuclear Energy*, *126*, 48-58. https://doi.org/https://doi.org/10.1016/j.anucene.2018.11.005

Skutnik, S. E., & Wieselquist, W. A. (2021). Assessment of ORIGEN Reactor Library Development for Pebble-Bed Reactors Based on the PBMR-400 Benchmark. https://doi.org/10.2172/1807271

Stewart, R., Balestra, P., Reger, D., Merzari, E., & Strydom, G. (2024). High-fidelity simulations of the run-in process for a pebble-bed reactor. *Annals of Nuclear Energy*, *195*, 110193. https://doi.org/https://doi.org/10.1016/j.anucene.2023.110193

Teuchert, E., Hansen, U., & Haas, K.-A. (1980). *VSOP-Computer code system for reactor physics and fuel cycle simulation*.

Wieselquist, W., & Lefebvre, R. A. (2023). *SCALE 6.3.1 User Manual*. https://www.osti.gov/biblio/1959594

Williams, M. L., Choi, S., & Lee, D. (2015). A new equivalence theory method for treating doubly heterogeneous fuel—I: theory. *Nuclear Science and Engineering*, *180*(1), 30-40. https://doi.org/https://doi.org/10.13182/NSE14-68